A terahertz view on magnetization dynamics

Awari, Nilesh

CHAPTER 5

THz-Induced Demagnetization: Case of CoFeB

Narrow band, tunable THz radiation is used to induce ultra-fast demagnetization in amorphous ferromagnetic thin films of CoFeB. The ultra-fast demagnetization is probed using the time resolved magneto-optical Kerr effect. We observe the non-monotonic frequency dependence of the ultra-fast demagnetization with a peak at $\sim$ 0.5 THz. This non-monotonic dependence is discussed using the Drude conductivity model and the Eliot-Yafet type scattering mechanism.

This chapter is based on a manuscript which is being prepared for a publication.
Awari N., et al. "Speed limits of ultra-fast demagnetization" *in preparation*

5.1 Introduction

The observation of ultra-fast demagnetization of nickel upon irradiation with near infrared (NIR) femtosecond (fs) laser pulses on sub-picosecond (sub-ps) timescale [1] initiated extensive research in the field of ultra-fast magnetization dynamics [2–8]. In laser induced ultra-fast magnetization dynamics, laser pulses heat electronic temperature above the Curie temperature on an ultra-fast timescale which results in loss of macroscopic spin order [9, 10]. The spin excitation in such experiments is an indirect process and it takes place by exchange of heat and angular momentum between the driving laser pulses, electrons, spins and lattice [11, 12]. The underlying physical mechanism explaining dissipation of the spin angular momentum on sub-ps timescale is still not clear.

There have been many different experimental and theoretical contributions to explain the dissipation of spin angular momentum on sub-ps timescale. Two major spin dissipation channels have been suggested:

1. The 3-temperature model (see chapter 2), based on the Elliot-Yaffet (EY) scattering mechanism, has been used to explain the ultra-fast demagnetization on the basis of spin-flip scattering. In this model ultra-fast demagnetization has been shown to be a thermal process, driven by the difference in the electronic, spin, and, lattice temperatures.

2. Alternatively, non-local spin transport, super-diffusive spin current[13–15], has been considered for spin dissipation. In this case, the energy and spin dependent lifetimes of optically excited hot electrons results in spin currents inside the material under investigation and that results in ultra-fast magnetization dynamics. There have been theoretical predictions suggesting super-diffusive spin current as the sole source of ultra-fast demagnetization[13, 16].

Reference [9] has shown that both spin-flip scattering and super-diffusive spin current plays an important role in ultra-fast magnetization. To date, the relative contributions of these two processes to the ultra-fast demagnetization is under debate.

Recently, THz radiation has been used to study ultra-fast magnetization dynamics in ferromagnetic systems [17–19]. As compared to NIR femtosecond driven ultra-fast demagnetization experiments, the use of the THz radiation allows the coupling of the spin system directly via the magnetic field component of the THz radiation. The THz pulses have been used to drive spin currents in magnetic metals [20]. When spin currents are generated, they undergo scattering events that changes the material magnetization. The THz pulse duration, being of the same order as elementary scattering rates, allows

to accurately model the influence of scattering events on material magnetization [17]. When compared with the optical excitation, in THz excitation of ferromagnetic materials, individual scattering events are more dominant than the relaxation of the highly non-equilibrium electronic system [17]. Bonetti et al. [17] have shown that ultra-fast demagnetization is detectable for amorphous CoFeB but not for crystalline Fe thin films. This hints towards defect mediated spin-lattice scattering. THz conductivity measurements on these thin films allowed the interpretation of these observations as Elliot-Yaffet [21, 17] type scattering processes. All of these experiments have made use of broadband THz radiation to study the ultra-fast demagnetization of the samples.

When strong THz pulses hit the ferromagnetic sample, spin-polarized current flows inside the sample which has two responses;

1. The coherent response can be explained using the Landau-Lifshitz equation. The magnetic field of the THz pump couples with the initial magnetization of the sample and results in precession. This magnetization dynamics can be explained using,

$$\frac{d\boldsymbol{M}}{dt} = -\gamma(\boldsymbol{M} \times \boldsymbol{H}) \tag{5.1}$$

   where γ is the gyro-magnetic ration with the value 28.02 GHz/T, $\boldsymbol{M}$ is the magnetization of the sample and $\boldsymbol{H}$ is the effective applied magnetic field. In the absence of a THz pulse, the sample magnetization is along the effective magnetic field comprising of anisotropy and demagnetizing fields. When a THz pulse passes through the sample, the magnetic field of the THz pulse ($\boldsymbol{B}_{THz}$) applies a torque on the sample magnetization which results in precession of the magnetization. For small angle precession, the magnetization can be given by [17],

$$M(t) = \gamma \sin\theta \int B_{THz}(t)dt \tag{5.2}$$

   where θ is an angle between M and H. This effect is odd in the magnetic field of the THz pulse. As we change the polarity of the B_{THz} by π, the sense of precession also reverses.

2. The incoherent response is a result of the spin-polarized current flowing through the sample because of the THz pulse inside the material. This effect is odd with respect to the magnetic field of the THz pulse [17]. The incoherent response can be modelled as a cumulative integral of the THz energy deposited in the sample [17], $\int B^2_{THz}(t)dt$.

In this chapter, tunable THz radiation is used as a non-resonant pump to excite the amorphous ferromagnetic thin films of CoFeB. This allows one to disentangle the spin to charge conversion processes at the THz frequencies with timescales which are similar to fundamental scattering rates.

5.2 Experimental details

The experimental set-up used in the experiment is shown in Figure 5.1. We used the narrow-band, tunable accelerator-based superradiant THz source, TELBE, to drive ultra-fast spin-polarized currents in an amorphous CoFeB thin film. The thin films were grown with sputtering with 5 nm thickness with a stack of Al_2O_3(2nm)/CoFeB(5nm) on silicon substrate. The peak electric field of the tunable THz radiation used were up to $\sim$ 100 kV/cm. The static magnetization of the sample was aligned in plane ($\boldsymbol{M_0}$) using a 100 mT permanent magnet, which is larger than the coercive field of CoFeB ($\sim$ 5 mT). Then we applied an external field of 100 mT perpendicular to the sample plane to bring the component of static magnetization out of the plane ($\boldsymbol{M}$). The magnetic field component of THz ($\boldsymbol{B}_{\mathrm{THz}}$) was aligned orthogonal to the magnetization of the sample (see Figure 5.2). The magnetization dynamics of the sample because of the THz-induced spin-polarized current was probed using THz pump 800 nm polar MOKE geometry. The ultra-fast magnetization response of the sample was recorded by taking the sum of the data taken at opposite polarities of the incident THz pump. In order to study the pump frequency dependence of the ultra-fast magnetization we made use of the tunability of the TELBE source.

The terahertz fields generated by TELBE are multicycle electromagnetic pulses with a center frequency tunable between 0.1 and 1.3 THz and with a bandwidth of approximately 20% (8 cycles) [22]. The electric field of these pulses can be measured through electro-optical (EO) sampling in a birifringent crystal such as ZnTe. An example of such a measurement is shown in Figure 5.3, where the EO sampling trace for two terahertz pulses with a center frequency of 0.5 THz and with opposite polarity is presented. Precise control of the phase of the terahertz radiation is achieved with suitable $\lambda/2$ wave-plates. In this experiment, we used the tunability of the TELBE source to study the incoherent response of magnetization as a function of THz pump frequency. Table 5.1 summarizes different THz pump frequencies used along-with its maximum electric field values.

At first we wanted to separate the coherent and incoherent responses of magnetization in CoFeB. In order to achieve that, we recorded the THz induced magnetization dynamics with opposite polarity of the THz pulse. As discussed earlier, the coherent response of

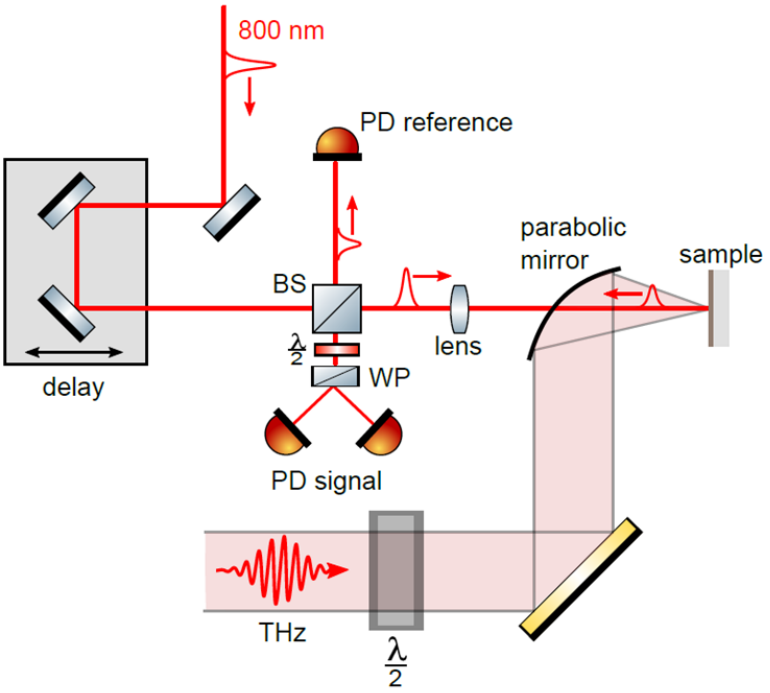

FIGURE 5.1: Experimental set-up used for narrow band THz pump MOKE probe measurements. A frequency tunable, narrow-band THz radiation (shown in light red band) is focused on the sample using a parabolic mirror. The NIR laser pulses (shown in red), which are synchronized to THz radiation, is incident colinearly on the samples. The transient change in sample magnetization is probed using the rotation of polarization of the NIR laser pulses using $\frac{\lambda}{2}$ (a half wave-plate for 800 nm), Wollaston prism (WP), and balanced photo-diodes (PD). A reference PD is used to monitor and normalize the reflected signal from the sample.

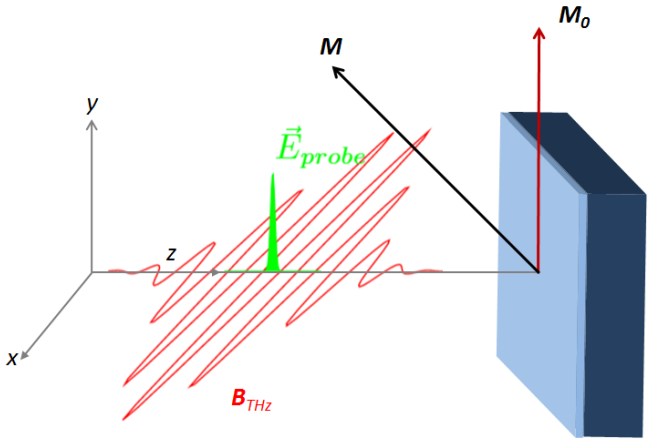

FIGURE 5.2: Experimental geometry used in the experiments. Initial magnetization of the sample ($\boldsymbol{M}_0$) is along the y axis and ($\boldsymbol{B}_{THz}$) is orthogonal to the initial magnetization.

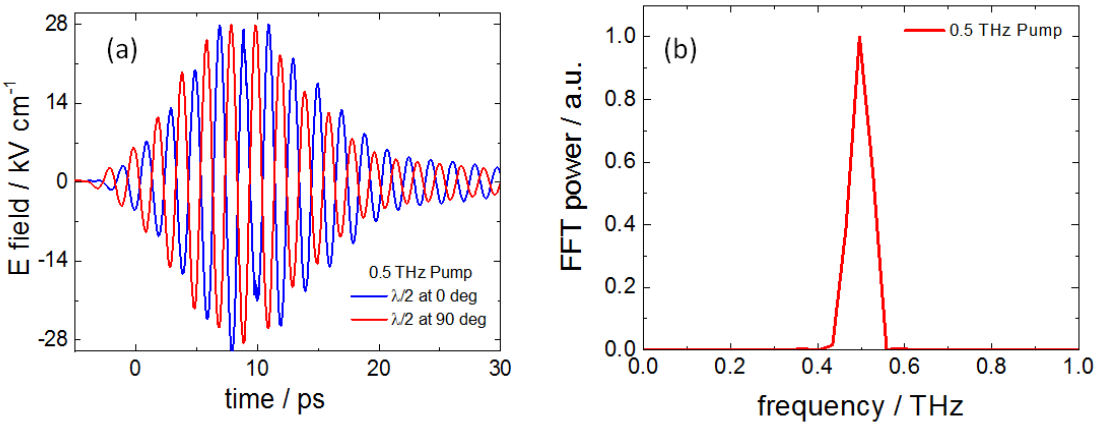

FIGURE 5.3: Time traces of the THz pump used in the experiment at 0.5 THz. (a) 0.5 THz time domain traces measured using electro-optic sampling in a 100 μm GaP detector at orthogonal half-wave plate angles (b) FFT of time trace for one of the HWP angles.

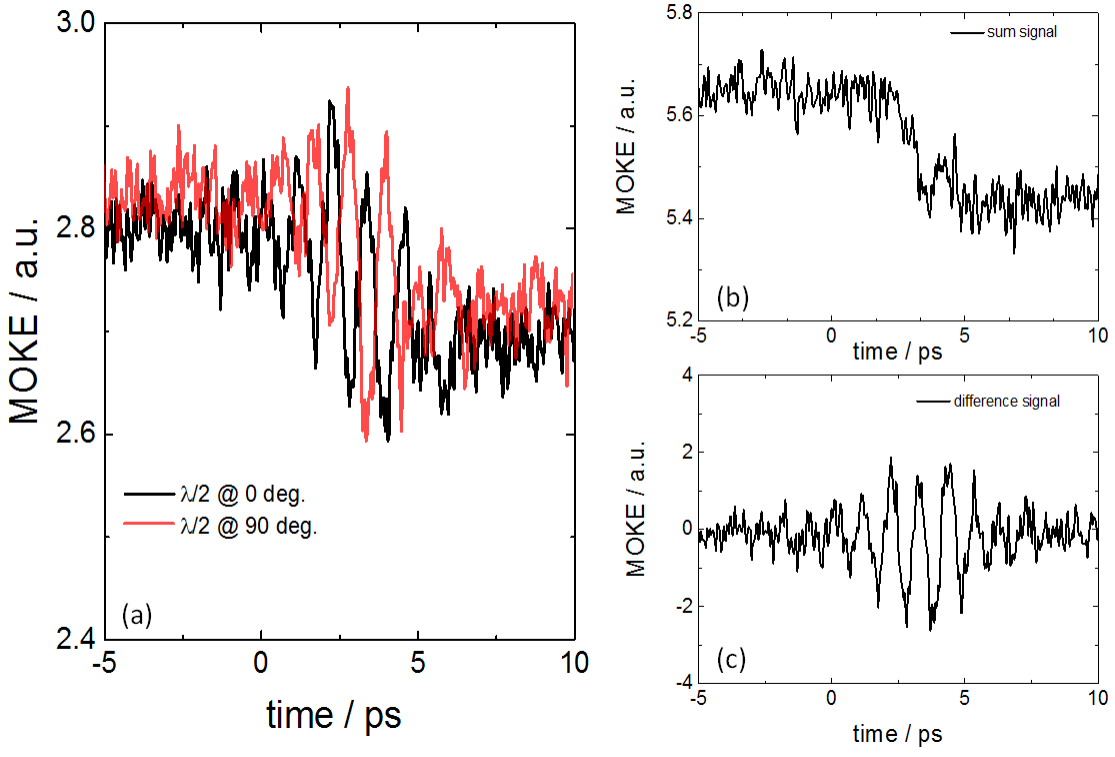

FIGURE 5.4: (a)THz pump time resolved MOKE signal observed in amorphous CoFeB thin films which includes the coherent and incoherent responses observed for opposite polarity of the THz electric/magnetic field. The frequency of the THz radiation used for this measurement was 1 THz with a focused spot size of 700 μm. (b) The incoherent response of the sample is obtained by taking the sum of the two curves shown in (a). (c)The coherent precession signal is separated from the incoherent one by taking the difference of the two curves shown in (a).

the magnetization is odd with respect to the magnetic field of the THz pulse, so it can easily be separated by subtracting the measurements done with opposite polarity of the THz pump. In contrast, addition of the measurements done with opposite polarity of the THz pump will only give the incoherent response of the magnetization. Figure 5.4 shows an example of the measured THz pump-MOKE signal for opposite THz pump polarity. It also shows how coherent and incoherent responses can be separated from each other.

Frequency (THz)	Electric field (kV/cm)
0.3	24
0.4	47
0.5	28
0.6	35
0.7	42
0.7	54.6
1	89
1	53

TABLE 5.1: A summary of the THz frequencies used in the THz pump Polar MOKE experiments along with their peak electric field values.

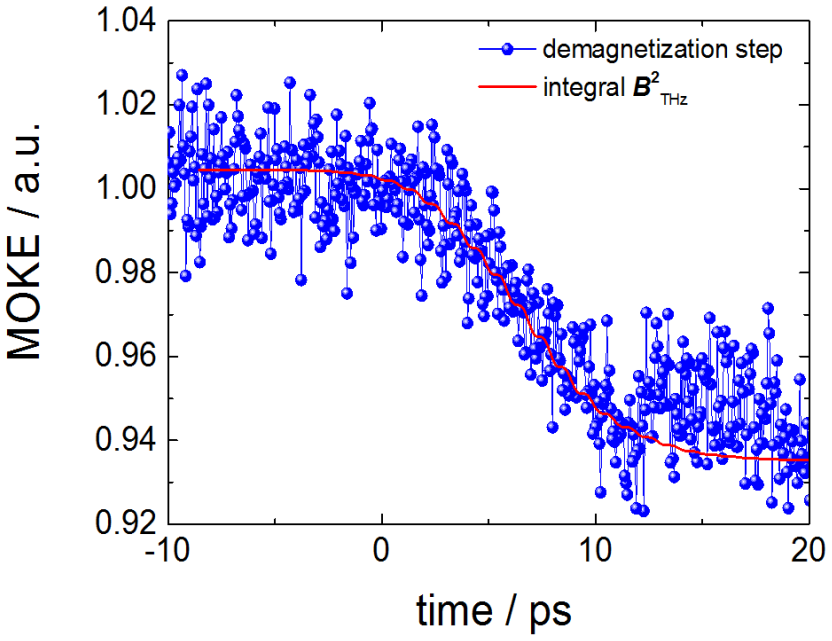

FIGURE 5.5: Ultra-fast demagnetization observed in CoFeB thin films with 0.5 THz pump is plotted in blue. The experimental data shows the second step in demagnetization around 10 picoseconds (ps). The integral of $\boldsymbol{B}_{THz}$ is plotted and shown in red. The cumulative integral does not follow the experimental data above 10 ps because reflections are not considered in the cumulative integral.

5.3 Results & Discussion

Figure 5.5 shows the incoherent response of the CoFeB thin film sample following the arrival of the terahertz pulse, as measured by the time-resolved MOKE with 0.5 THz as a pump and showing that the sample demagnetizes while the THz pulse is present in the sample. This is consistent with the results of Refs.[17, 18], with the important difference that in those works the excitation was a broadband terahertz pulse, while here we use narrow-band radiation. However, the magnetization dynamics is based on the very same mechanism: the coherent response can be modeled as the integral of B_{THz}, showing it obeys the Landau Lifshitz Gilbert (LLG) equation; the incoherent response is modelled by the cumulative integral of B_{THz}^2, i.e. by the energy deposited by the terahertz field in the material.

In Figure 5.5, we also observe two steps in the demagnetization data. The observed second step is believed to be because of the reflection of the THz pulse from the back surface of the substrate. The time delay between the two steps (approximately 10 ps) is consistent with the optical path traveled in a 500 μm thick silicon substrate ($n \approx 3.41$). In order to compare the demagnetization step as a function of the THz pump, we consider the first step, as it is not influenced by the reflected THz pulse from the back surface of the substrate. The modelled cumulative integral does not follow the experimental data after 10 ps because we do not consider reflections in the cumulative integral.

In Figure 5.6 the demagnetization step as a function of THz pump power is plotted. We observe the linear relation between the demagnetization step and THz pump power which is expected for the energy dissipation because of the scattering in THz induced spin current [17].

In order to probe the complete coherent response initiated by the THz pump, one needs to scan longer as the ferromagnetic resonance (FMR) of CoFeB can be seen on nanosecond timescales. In TELBE, one can probe the dynamics on longer timescales by delaying the phase between the probe laser and the accelerator master-clock by electronic means. Figure 5.7 shows the FMR observed for CoFeB, initiated after the initial demagnetization.

Similar ultra-fast demagnetization scans were measured for different THz pump frequencies, with electric field values summarized in Table 5.1. The tunable and narrow-band excitation measurements allows one to study the ultra-fast demagnetization as a function of excitation frequency and allows us to measure the efficiency of the ultra-fast demagnetization directly. In Figure 5.8, the demagnetization steps observed for two different THz pump frequencies (0.7 THz and 1 THz) are plotted. In order to compare

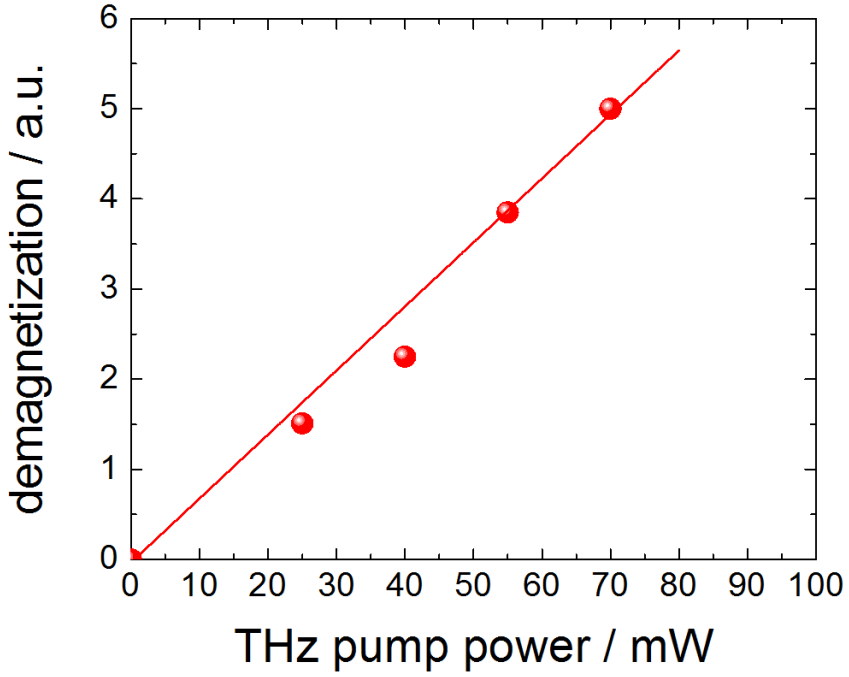

FIGURE 5.6: Ultra-fast demagnetization observed in CoFeB thin films with THz pump as a function of pump power.

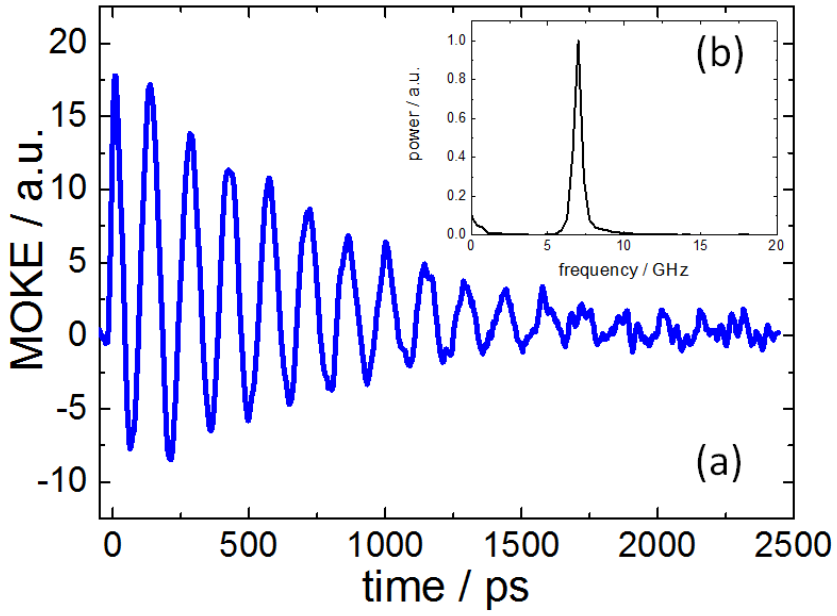

FIGURE 5.7: The initiated incoherent demagnetization leads to the excitation of the ferromagnetic resonance on nanosecond timescales in CoFeB thin films. (a) the time-domain scan of the FMR mode in CoFeB (b) Fourier transform of the time-domain scan showing the FMR mode of roughly 7 GHz.

these two curves, we normalize these demagnetization curves with the square of the electric field used as a pump. The normalization factor used here gives the amount of energy deposited inside the material by the THz excitation. Upon normalization, we observed that demagnetization step is frequency dependent and, at 0.7 THz pump, the demagnetization step is larger than one at 1 THz. The 0.7 THz pump scan looks noisier than the one at 1 THz because of the different normalization factors used.

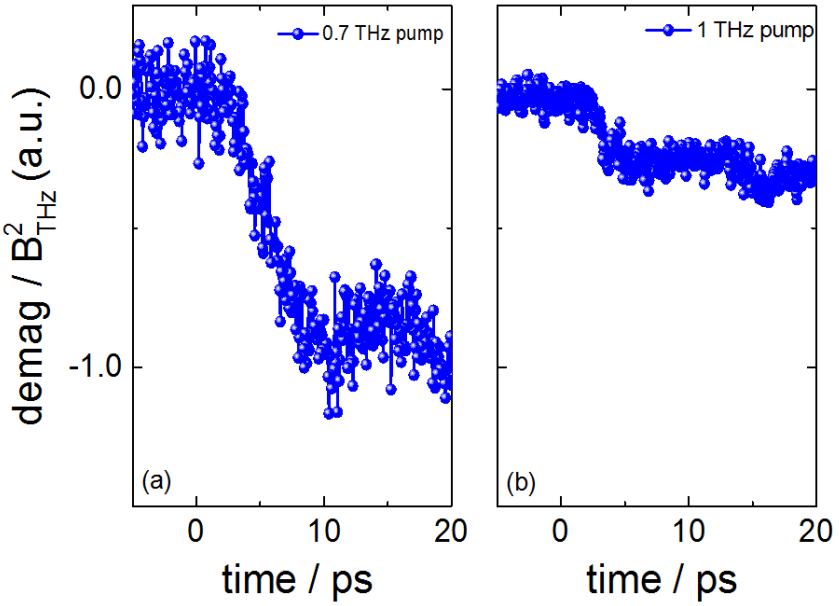

FIGURE 5.8: Ultra-fast demagnetization observed in CoFeB thin films (a) with 0.7 THz pump and (b) 1 THz pump. The demagnetization step is lower at 1 THz pump as compared to demagnetization at 0.7 THz. The noise floor for the 1 THz scan looks smaller than at 0.7 THz because of the normalization with respect to B^2_{THz}.

Figure 5.10 shows the normalized ultra-fast demagnetization observed in CoFeB thin films over two different TELBE beam-times, taken 6 months apart. In this figure, we see that demagnetization of CoFeB thin films shows non-monotonous dependence on THz pump frequency with a peak observed at 0.5 THz. The error bar in the THz frequency is taken as the bandwidth of the TELBE source (20%). The error in the demagnetization step is calculated by taking the standard deviation of the measurement points before time zero, within 1 σ interval. The data point at 0.7 and 0.4 THz has a larger error bar. This larger error bar could be because of systematic errors in the measurements. This systematic error could be because of having slightly different THz pump frequency in different beam-times. The error in such cases is calculated using the following equation;

$$\delta(\Delta M) = (\delta(\Delta M_1)^2 + \delta(\Delta M_2)^2 + (\delta(syst))^2)^{1/2} \tag{5.3}$$

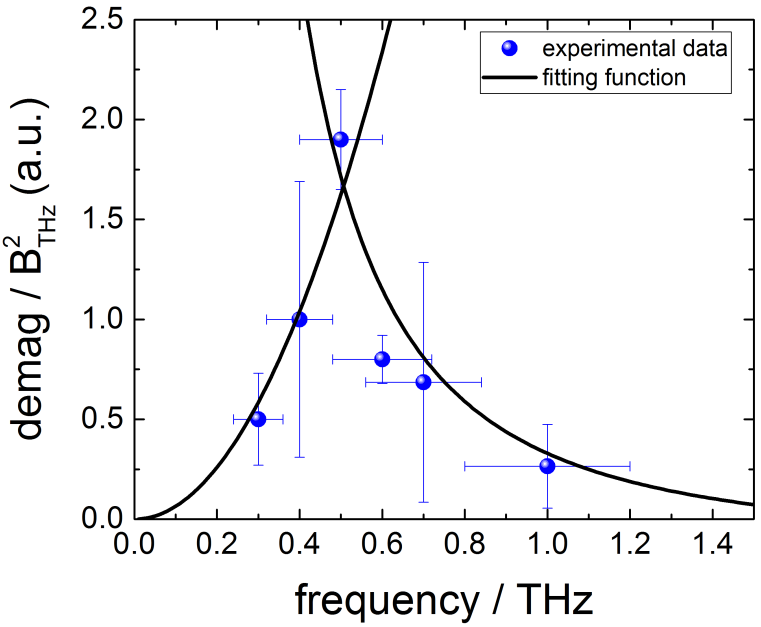

FIGURE 5.9: Ultra-fast demagnetization observed in CoFeB thin films as a function of the THz pump frequency. The error bars are explained in the text. Modelling of the frequency dependence of the THz induced demagnetization in CoFeB is done using two competing mechanisms; Eliot-Yafet type spin-flip scattering and Drude conductivity model (black line).

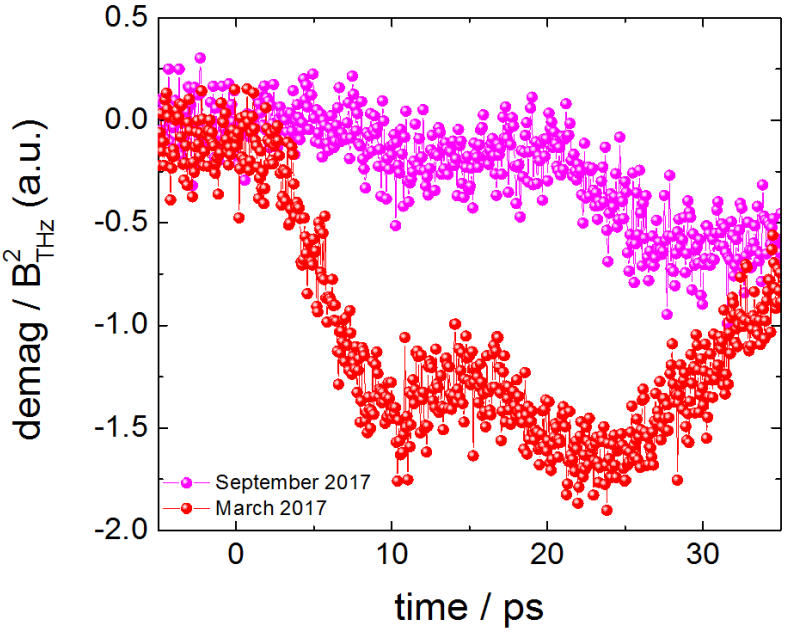

FIGURE 5.10: Ultra-fast demagnetization observed in CoFeB thin films at 0.7 THz pump. Red data points were measured during March 2017 TELBE beam-time whereas magenta data points were measured during September 2017 beam-time.

Here $\delta(\Delta M_1)$ and $\delta(\Delta M_2)$ is calculated by taking the standard deviation of the measurements points before time zero and $\delta(syst)$ is the difference in demagnetization observed in two different beam-times. In order to explain the non-monotonic dependence of demagnetization on THz pump frequency, we propose the following mechanisms.

The first mechanism is based on an assumption that defect-driver Eliot-Yafet spin flip scattering events are the cause for demagnetization in the thin film [17]. Following the Drude model for free electrons [23, 24], the average distance travelled by a conduction electron when THz field is applied to the sample is;

$$x(t) = eE(t)/m\omega^2 \tag{5.4}$$

where *E(t)* is an applied electric field, e is the electronic charge and ω is the angular frequency of the THz pulse, and m is the free electron mass. It corresponds to the mean free path for electric field of infinite duration. When electron travels because of the sinusoidal electric field, it gets scattered from the defect site. This scattering will result in spin-flip and thus in demagnetization (ΔM). The magnitude of ΔM can be estimated from,

$$\Delta M = P_{sf} N(\epsilon \frac{\mu_B}{2e}) \tag{5.5}$$

where P_{sf} is spin-flip scattering probability and N is the number of scattering events which will be proportional to distance travelled by an electron and the density of defects. Factor $\epsilon \frac{\mu_B}{2e}$ is spin to charge conversion factor with μ_B is Bohr magneton and ϵ is spin polarization of the material.

The total number of scattering events during time t for which THz electric field is applied to the sample can be estimated using;

$$N = \int_0^t \frac{x(t)}{x_{defects}} I(\zeta) d\zeta \tag{5.6}$$

where *x(t)* is average distance travelled by conducting electrons because of the electric field (E), given by equation 5.4, x_{defect} is the average distance between the defects, and integral gives the current flowing inside the material in the presence of the THz pulse. Combining equation 5.5 and 5.6 one can write;

$$\Delta M \sim \rho_{\text{defects}} \frac{E^2(t)}{\nu^2} \tag{5.7}$$

Here, $\rho_{defects} = 1/x_{def}$ is the density of the defects and $\nu = \omega/2\pi$. This equation shows that the magnetization is dependent on the density of defects and the square of the THz field, as observed in ref. [17] and as shown in Figure 5.6. Above equation shows that the demagnetization of the material will increase as the the frequency of excitation has decreased. This can be understood as the frequency of THz pump is decreased, the time for which an electron is travelling is larger making it more susceptible for spin-flip scattering. This will result in increased demagnetization as the THz pump frequency is decreased. With this mechanism one can predict the high frequency response demagnetization observed in CoFeB (above 0.5 THz), see Figure 5.9.

The decrease in demagnetization at lower frequencies is still debated and here two possible mechanisms are considered. At first the effect of frequency on the efficiency of EY mechanism considered. In EY mechanism the spin scattering rate (Γ_s) is proportional to momentum scattering rate (Γ) [25, 26];

$$\Gamma_s \propto \Gamma \tag{5.8}$$

The Fermi liquid theory, where interacting electrons are considered, predicts the momentum scattering rate to be [27];

$$\Gamma \sim (E - E_F)^2 \tag{5.9}$$

where $(E - E_F)$ is the energy of the accelerated electrons because of the THz electric field and E_F is the Fermi energy. The above equation is valid for weakly interacting electrons with energy of electrons being very close to the Fermi surface. The energy provided by the THz excitation is few meV as compared to few eV for the Fermi energy of the system considered here. Considering equations 5.8 and 5.9, one can predict that the spin scattering rate (Γ_s) scales with the square of the energy of the free electron. In this experiment, the spin scattering rate (Γ_s) is proportional to the demagnetization observed in the material, which predicts the demagnetization to scale with the square of the THz frequency used for excitation.

$$P_{sf} \sim \nu^2 \tag{5.10}$$

Combining equations 5.7 and 5.10, one can predict the occurrence of the peak in the frequency dependence of the demagnetization (see Figure 5.9). In Figure 5.9, two functions are used to fit the high frequency data points and low frequency data points. The

exact relation and dependence of these two functions on each other is not yet clear and would form the basis for future experiments.

Another approach to describe the peak behavior in the Figure 5.9 is based on attempts to form universal spin-relaxation theory. Spin-relaxation is generally defined using two different mechanisms with and without inversion symmetry of the system under consideration. The Elliot-Yafet (EY) mechanism is applied for materials with inversion symmetry where as Dyakonov-Perel mechanisms (DY) is applied for materials which lacks inversion symmetry. Recently it has been shown that EY and DP are closely related and each mechanism can be derived in the framework of the other mechanism [28]. In this article authors have suggested a practical and simpler numerical way to calculate the spin scattering rate. The universal function to calculate the spin scattering rate is [28],

$$\Gamma_s(\Gamma) \sim \Gamma/(1+\Gamma^2) \tag{5.11}$$

here Γ_s and Γ are measured in the units of spin orbit energies. This equation correctly predicts the peak in spin scattering rate as a function of momentum scattering rates but only qualitatively for the experiment discussed in this chapter. One of the key features of this function is smooth decay at higher frequencies whereas for the current experiment we observe sharp decay at higher frequencies.

Another mechanism to understand the lowering of demagnetization at lower frequency is based on the atomistic re-magnetization model [29]. A microscopic model, based on a 3 temperature model (3TM), has been proposed to explain the thermal recovery of the magnetization. In this article, authors have shown a non-monotonic temporal evolution of atomic moments and the macroscopic re-magnetization. The timescale involved in such calculations are of the order of picosecond to nanosecond [2, 29]. In the current experiment, as the frequency of THz pump is lowered, the amount of time for which spin-polarized current flows inside the material increases. At sufficiently lower frequencies, the time for which spin-polarized current flows may become longer than the timescale of the re-magnetization process. But in the current experiment, the timescale involved is faster than the one predicted for re-magnetization in ref.[29] and therefore this mechanism is not considered to explain the non-monotonous dependence of demagnetization on the THz frequency.

In order to support the claim on the effect of defects/scatterers on the ultra-fast demagnetization of the sample, new thin films of CoFeB (20 nm) were grown and implanted with platinum (Pt) and copper (Cu). The implantation of different elements in pristine

CoFeB increases the number of defects in it. The defects with stronger spin-orbit coupling and spin-scattering probability will enhance the spin-flip scattering and may result in higher demagnetization. Two different elements were chosen for implantation because of their different spin-orbit strengths. Pt-implanted films are believed to be more effective for spin-flip scattering because of its higher spin-orbit coupling as compared to Cu ones. Figure 5.11 shows the demagnetization observed at 1 THz pump for different samples. One can clearly see that Pt implanted CoFeB shows higher demagnetization as compared to pristine CoFeB and Cu implanted CoFeB for same the thicknesses. When the demagnetization of 20 nm thin films were compared with 5 nm films (Figure 5.11, red dot), one observes that demagnetization is roughly 4 times higher for 5 nm thin films as compared to 20 nm films. We believe that the reason for smaller demagnetization in thicker films is because of the lower conductivity of the films.

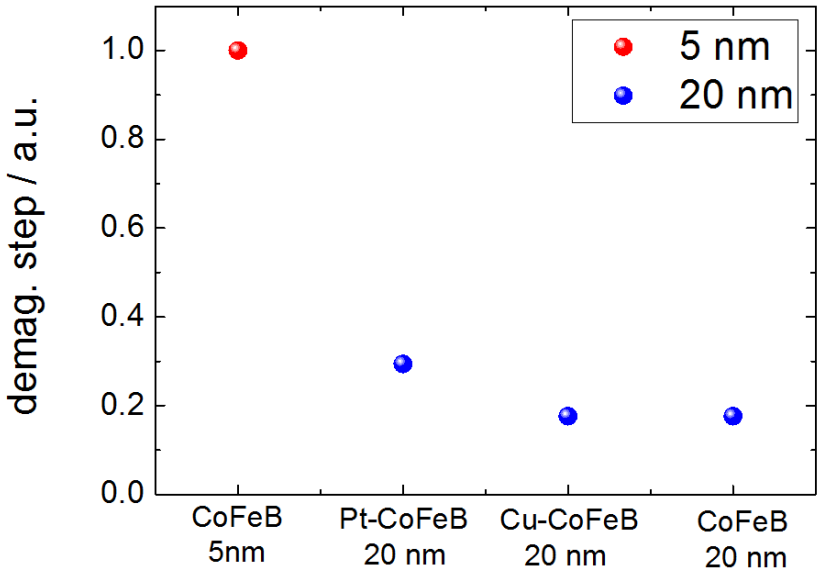

FIGURE 5.11: Comparison of normalized demagnetization efficiency at 1 THz for pristine CoFeB (5 nm, red dot), pristine CoFeB, Pt-CoFeB, and Cu-CoFeB. The THz spot size was roughly 700 μm with electric field of 89 kV/cm.

5.4 Conclusion & Outlook

THz induced ultra-fast demagnetization is studied for amorphous CoFeB thin films. We observe the non-monotonic frequency dependence of ultra-fast demagnetization. To explain the non-monotonus frequency dependence we propose the mechanism which is a competition between Eliot-Yafet type scattering spin-flip mechanism and scattering of the conducting electrons in Drude model. In order to support the Drude conductivity

model for ultra-fast demagnetization, we implanted CoFeB thin films with different elements to introduce the defects. The implanted samples with Pt implantation showed higher demagnetization as compared with pristine, supports the claim of spin-flip scattering because of higher spin-orbit coupling introduced by Pt implantation.

This study provides an experimental tool to understand the physics of fundamental scattering rates as a function of THz frequency at sub-picosecond timescales. To understand our experimental work better, a new theoretical framework is expected to be developed. Our experimental findings will pave the way for new experimental work to develop a microscopic understanding of ultra-fast magnetization dynamics. This will allow one to design efficient data storage devices for technological applications.

5.5 Bibliography

[1] E. Beaurepaire, J.-C. Merle, A. Daunois, and J.-Y. Bigot, "Ultrafast spin dynamics in ferromagnetic nickel," *Physical review letters*, vol. 76, no. 22, p. 4250, 1996.

[2] B. Koopmans, J. Ruigrok, F. Dalla Longa, and W. De Jonge, "Unifying ultrafast magnetization dynamics," *Physical review letters*, vol. 95, no. 26, p. 267207, 2005.

[3] C. Stamm, T. Kachel, N. Pontius, R. Mitzner, T. Quast, K. Holldack, S. Khan, C. Lupulescu, E. Aziz, M. Wietstruk, *et al.*, "Femtosecond modification of electron localization and transfer of angular momentum in nickel," *Nature materials*, vol. 6, no. 10, p. 740, 2007.

[4] F. Dalla Longa, J. Kohlhepp, W. De Jonge, and B. Koopmans, "Influence of photon angular momentum on ultrafast demagnetization in nickel," *Physical Review B*, vol. 75, no. 22, p. 224431, 2007.

[5] E. Carpene, E. Mancini, C. Dallera, M. Brenna, E. Puppin, and S. De Silvestri, "Dynamics of electron-magnon interaction and ultrafast demagnetization in thin iron films," *Physical Review B*, vol. 78, no. 17, p. 174422, 2008.

[6] B. Koopmans, M. Van Kampen, J. Kohlhepp, and W. De Jonge, "Ultrafast magneto-optics in nickel: magnetism or optics?," *Physical Review Letters*, vol. 85, no. 4, p. 844, 2000.

[7] C. Boeglin, E. Beaurepaire, V. Halté, V. López-Flores, C. Stamm, N. Pontius, H. Dürr, and J.-Y. Bigot, "Distinguishing the ultrafast dynamics of spin and orbital moments in solids," *Nature (London)*, vol. 465, p. 458, 2010.

[8] A. Kirilyuk, A. V. Kimel, and T. Rasing, "Ultrafast optical manipulation of magnetic order," *Reviews of Modern Physics*, vol. 82, no. 3, p. 2731, 2010.

[9] T. Roth, A. Schellekens, S. Alebrand, O. Schmitt, D. Steil, B. Koopmans, M. Cinchetti, and M. Aeschlimann, "Temperature dependence of laser-induced demagnetization in ni: A key for identifying the underlying mechanism," *Physical Review X*, vol. 2, no. 2, p. 021006, 2012.

[10] J.-Y. Bigot, M. Vomir, and E. Beaurepaire, "Coherent ultrafast magnetism induced by femtosecond laser pulses," *Nature Physics*, vol. 5, no. 7, p. 515, 2009.

[11] G. Zhang, W. Hübner, G. Lefkidis, Y. Bai, and T. F. George, "Paradigm of the time-resolved magneto-optical kerr effect for femtosecond magnetism," *Nature physics*, vol. 5, no. 7, p. 499, 2009.

[12] K. Carva, M. Battiato, and P. M. Oppeneer, "Is the controversy over femtosecond magneto-optics really solved?," *Nature Physics*, vol. 7, no. 9, p. 665, 2011.

[13] M. Battiato, K. Carva, and P. M. Oppeneer, "Superdiffusive spin transport as a mechanism of ultrafast demagnetization," *Physical review letters*, vol. 105, no. 2, p. 027203, 2010.

[14] K. Carva, M. Battiato, D. Legut, and P. M. Oppeneer, "Ab initio theory of electron-phonon mediated ultrafast spin relaxation of laser-excited hot electrons in transition-metal ferromagnets," *Physical Review B*, vol. 87, no. 18, p. 184425, 2013.

[15] D. Rudolf, L.-O. Chan, M. Battiato, R. Adam, J. M. Shaw, E. Turgut, P. Maldonado, S. Mathias, P. Grychtol, H. T. Nembach, *et al.*, "Ultrafast magnetization enhancement in metallic multilayers driven by superdiffusive spin current," *Nature communications*, vol. 3, p. 1037, 2012.

[16] M. Battiato, K. Carva, and P. M. Oppeneer, "Theory of laser-induced ultrafast superdiffusive spin transport in layered heterostructures," *Physical Review B*, vol. 86, no. 2, p. 024404, 2012.

[17] S. Bonetti, M. Hoffmann, M.-J. Sher, Z. Chen, S.-H. Yang, M. Samant, S. Parkin, and H. Dürr, "Thz-driven ultrafast spin-lattice scattering in amorphous metallic ferromagnets," *Physical review letters*, vol. 117, no. 8, p. 087205, 2016.

[18] M. Shalaby, C. Vicario, and C. P. Hauri, "Low frequency terahertz-induced demagnetization in ferromagnetic nickel," *Applied Physics Letters*, vol. 108, no. 18, p. 182903, 2016.

[19] M. Shalaby, C. Vicario, and C. P. Hauri, "Simultaneous electronic and the magnetic excitation of a ferromagnet by intense THz pulses," *New Journal of Physics*, vol. 18, no. 1, p. 013019, 2016.

[20] Z. Jin, A. Tkach, F. Casper, V. Spetter, H. Grimm, A. Thomas, T. Kampfrath, M. Bonn, M. Kläui, and D. Turchinovich, "Accessing the fundamentals of magnetotransport in metals with terahertz probes," *Nature Physics*, vol. 11, no. 9, p. 761, 2015.

[21] B. Koopmans, G. Malinowski, F. Dalla Longa, D. Steiauf, M. Fähnle, T. Roth, M. Cinchetti, and M. Aeschlimann, "Explaining the paradoxical diversity of ultrafast laser-induced demagnetization," *Nature materials*, vol. 9, no. 3, p. 259, 2010.

[22] B. Green, S. Kovalev, V. Asgekar, G. Geloni, U. Lehnert, T. Golz, M. Kuntzsch, C. Bauer, J. Hauser, J. Voigtlaender, *et al.*, "High-field high-repetition-rate sources for the coherent THz control of matter," *Scientific reports*, vol. 6, p. 22256, 2016.

[23] P. Drude, "Zur elektronentheorie der metalle," *Annalen der Physik*, vol. 306, no. 3, pp. 566–613, 1900.

[24] D. J. Griffiths, "Electrodynamics," *Introduction to Electrodynamics, 3rd ed., Prentice Hall, Upper Saddle River, New Jersey*, pp. 301–306, 1999.

[25] R. . J. Elliott, "Theory of the effect of spin-orbit coupling on magnetic resonance in some semiconductors," *Physical Review*, vol. 96, no. 2, p. 266, 1954.

[26] H. Ochoa, A. C. Neto, and F. Guinea, "Elliot-Yafet mechanism in graphene," *Physical review letters*, vol. 108, no. 20, p. 206808, 2012.

[27] N. W. Ashcroft and N. D. Mermin, "Solid state physics," *Harcourt College Publishers*, p. 461, 1976.

[28] L. Szolnoki, B. Dóra, A. Kiss, J. Fabian, and F. Simon, "Intuitive approach to the unified theory of spin relaxation," *Physical Review B*, vol. 96, no. 24, p. 245123, 2017.

[29] R. Chimata, A. Bergman, L. Bergqvist, B. Sanyal, and O. Eriksson, "Microscopic model for ultrafast remagnetization dynamics," *Physical review letters*, vol. 109, no. 15, p. 157201, 2012.